


Atom Classification Model for Total Energy Evaluation of Two-Dimensional Multicomponent Materials

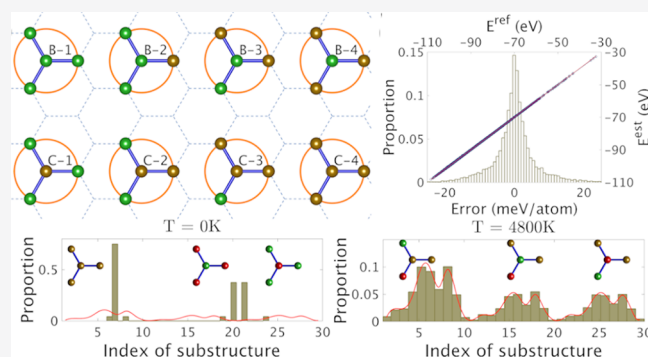
Chang-Chun He, Shao-Bin Qiu, Ju-Song Yu, Ji-Hai Liao, Yu-Jun Zhao, and Xiao-Bao Yang*

 Cite This: *J. Phys. Chem. A* 2020, 124, 4506–4511 Read Online

ACCESS |

 Metrics & More Article Recommendations

ABSTRACT: The tunable properties of materials originate from variety of structures; however, it is still a challenge to give an accurate and fast evaluation of stabilities for screening numerous candidates. Herein, we propose an atom classification model to describe the multicomponent materials based on the structural recognition, in which the atoms are classified to estimate the total energies. Taking two-dimensional planar $C_{1-x}B_x$ and $C_{1-2x}(BN)_x$ as examples, we have found that the test error of total energies is about 3 meV per atom. Notably, the distributions of classified atoms demonstrate the evolution of configurations as a function of temperature, providing a clearer picture of phase transition. In addition, our method is universal, which can be flexibly extended to the bulk structures with more components.



INTRODUCTION

The properties of materials depend on the dimension of materials and local distribution of corresponding atoms.^{1–3} Novel physical phenomena have been revealed in low-dimensional materials because graphene was peeled off,⁴ such as the quantum spin Hall effect^{5,6} and two-dimensional (2D) superconductivity.^{7,8} In addition to the dimension reduction, alloy engineering⁹ is another important avenue to explore new materials under ambient conditions. Boron–carbon binary alloy and boron–carbon–nitride (BCN) ternary alloy show wide variety of physical and chemical properties because of the variety of structures.^{10–12} Recent experiments focused on 2D hexagonal graphene-like structures, such as the heterostructures of graphene and hexagonal boron nitride.¹³ On the substrate of Ru(0001), the order–disorder phase transition was observed in 2D BCN alloy.¹⁴

Theoretically, the first-principles calculations based on density functional theory (DFT)¹⁵ are powerful to predict the properties of materials accurately and accelerate the discovery of new materials greatly.^{16–18} However, it is difficult to directly simulate all possible configurations of multicomponent materials using the DFT calculations because of numerous isomers. To describe structural stabilities, cluster expansion (as implemented in ATAT¹⁹) is an effective method to construct the model Hamiltonian with the accuracy of the DFT calculations, where the selection of leading parameters is important to predict the unknown ground states.²⁰ With the total energies from cluster expansion combined with first-principles calculations, the phase diagram of BCN monolayers has been studied by the Monte Carlo simulation.²¹ Theoretical

predictions showed that most of $C_{1-2x}(BN)_x$ structures possess direct band gaps within the optical range, which can potentially be used in the solar-cell device with high-efficiency conversion.²² In addition, zigzag boron nitride nanoribbons with edge functionalization have been found to be the potential new nanoelectronic and nanospintronic devices because of their half-metallic states.²³

In general, total energies and other properties can be correlated with the sampling configurations to determine the parameterized model by minimizing the fitting error while the parameters in the model are hardly corresponded to any quantity in the DFT calculations. In this paper, we have developed an atom classification model (ACM) to describe the structural stabilities for $C_{1-x}B_x$ and $C_{1-2x}(BN)_x$ hexagonal structures, where the test error of total energies is about 3 meV per atom. The parameters in the model can be reflected by the charge distributions as an evidence to show the physical connotation, according to which the number of parameters can be reduced without remarkably decreasing the accuracy. In addition, the probability distributions of motifs show a direct picture of the configuration evolution as a function of temperature, serving as the role of order parameters.

Received: March 19, 2020

Revised: May 6, 2020

Published: May 6, 2020



METHOD

The main idea of ACM is to classify each atom based on its neighboring configurations, which is countable because the atoms are initially at the *lattice sites*. Taking the graphene doped by a boron (B) atom as an example, the Hirshfeld analysis²⁴ indicates that the charge on carbon (C) atoms far away the B atom is $4.00e$, which is the same as in the pure graphene, while the charges are $4.18e$ and $3.95e$ for carbon atoms at the nearest neighboring (NN) and next-NN (NNN) to the B atom (shown in Figure 1a). When doped by three B

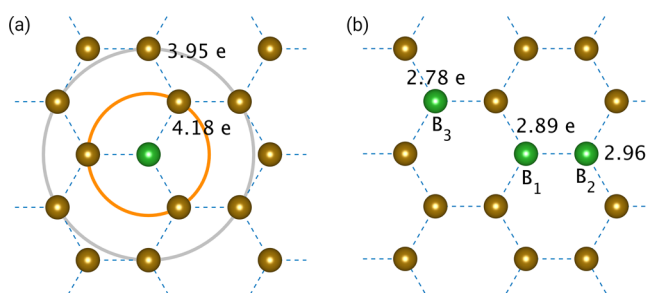


Figure 1. Hirshfeld charge at some specific atoms in boron-doped graphene: (a) BC_{71} , (b) B_3C_{69} . The C and B atoms are marked with golden and green, respectively. The orange and gray circles represent the NN and NNN regions, respectively.

atoms shown in Figure 1b, the NN bonding configurations of B_1 and B_2 are the same, but the charges are $2.89e$ and $2.96e$ because there are all carbon atoms for B_2 while there is one boron atom for B_1 at the NNN site. In multicomponent materials, the total energies and electronic properties depend on the charge distribution, which is determined by the configuration of atomic local bonding. With the concept of

“environment”, all the interactions within the cut-off radius are included, and the total energies can be expressed by the summation of all atomic contribution. Note that the charge distribution can be preclassified by the local bonding configurations based on the lattice symmetry, where the cut-off radius for the classification should be tested according to the fitting error.

We have performed a high-throughput first-principles calculations based on the structural recognition, focusing on $C_{1-x}B_x$ and $C_{1-2x}(BN)_x$ monolayers. For the given structures, the first-principles calculations were performed using the Vienna Ab initio Simulation Package (VASP).^{25,26} The projector-augmented plane wave approach²⁷ was adopted with the Perdew–Burke–Ernzerhof of generalized gradient approximation functional.²⁸ The energy cutoff of the plane wave was 480 eV, and the criteria of the energies convergence were set to be 0.001 eV in self-consistent calculations. The Brillouin zone was sampled with allowed spacing between k points in 0.2 \AA^{-1} , with Γ -centered Monkhorst–Pack k -point grid for high-throughput calculations. For the stable structures with specific properties, the atomic positions and lattice constants are fully relaxed, until the forces were less than 0.02 eV/\AA .

To maintain the structural diversity of candidates, we have enumerated $C_{1-x}B_x$ and $C_{1-2x}(BN)_x$ monolayers with various atomic compositions and distributions, using the package of Structures of Alloy Generation And Recognition (SAGAR)²⁹ developed in our group. The possible supercells with given sizes can be generated using hermite normal form matrices,³⁰ where the unique supercells are kept according to the congruence check. With a given supercell, all the isomers with possible compositions are also enumerated, and the unique configurations are generated based on the structural

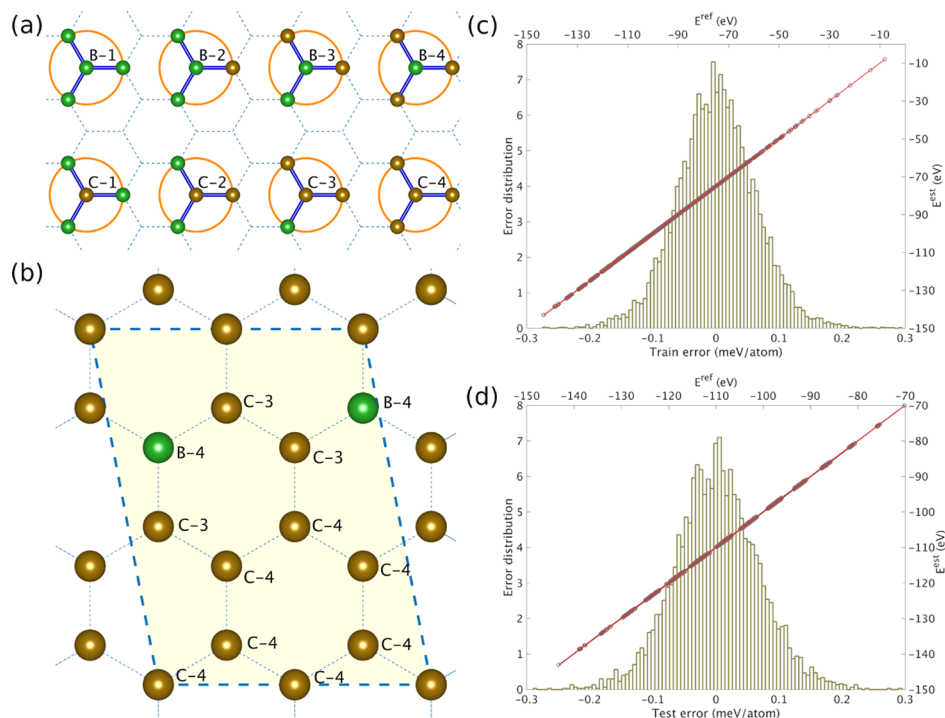


Figure 2. Atom classification for total energies: (a) Eight kinds of atomic motifs for the NN cut-off; (b) an example of boron-doped graphene with possible kinds of atomic motifs. The test error distribution, as well as the consistency of E^{est} predicted by the model and E^{ref} from the DFT calculations of (c) $C_{1-x}B_x$ and (d) $C_{1-2x}(BN)_x$.

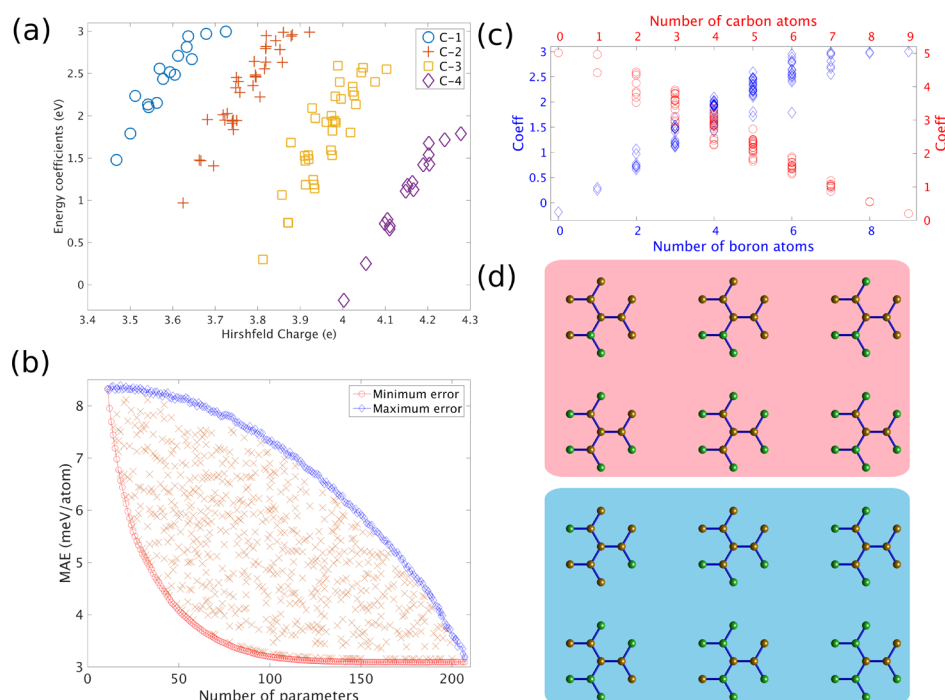


Figure 3. Atom classifications for fitting total energies: (a) the parameters as a function of charges; (b) Monte Carlo tree search for the key classifications; (c) the parameters of B/C-centered motifs as a function of C/B atoms in various motifs; (d) C-centered motifs, with the most/least stable ones marked in blue/red background.

recognition. Our previous studies showed that the structural recognition can be achieved by either the distance matrices³¹ or the symmetry operation table.³²

RESULTS AND DISCUSSION

Following the procedure of ACM, the energies of possible candidates are the linear contributions of atomic motifs with various bonding environments, expressed as: $E = \sum_{i=1}^{N_m} \alpha_i \epsilon_i$, where ϵ_i is the contribution of i -th motif, α_i is the number of i -th motif in the structure, and N_m is the number of possible motifs. For the B-doped graphene, we can divide the atoms into two kinds, that is, B and C, when the neighboring environments are not considered. As shown in Figure 2a, there are eight kinds of unique atoms, when the cut-off radius is set to nearest neighbors while the number of kinds is 208 with the cut-off radius up to next-nearest neighbors. To optimize the energy parameters, we have performed the first-principles calculations of 17 010 $C_{1-x}B_x$ ($0 \leq x \leq 1$) monolayer configurations (an example with the classified atoms shown in Figure 2b), including the supercells of hexagonal lattice with the unit cell sizes from 1 to 8. To avoid the overfitting, the L^2 regularization³³ is adopted with the matrix form of regression:

$$f(\epsilon) = \frac{1}{2} \|A\epsilon - E\|^2 + \frac{\lambda}{2} \|\epsilon\|^2$$
, where λ is the suitable regularization parameter and A is the 2D matrix whose each row is the identification of monolayers. Minimizing $f(\epsilon)$, the optimum parameter ϵ is $\epsilon = (A^T A + \lambda I)^{-1} A^T E$, which can be solved by the gradient descent algorithm or least angle regression algorithm, if the size of A is large.

In order to get the proper model parameters, we take 70% data as the train set to obtain ϵ with regular parameter $\lambda = 0.01$, and the remnant data are test set to verify our model. Figure 2c shows that the train error and test error are 3.05 and 3.25 meV/atom, respectively, indicating the good accuracy of

our model Hamiltonian. Furthermore, the test error will be 3.91 (3.37) meV/atom, if we take 10% (40%) data for training and the remnant data for testing, demonstrating the robustness of this model. Additionally, we have performed the similar calculations on the 15 840 $C_{1-2x}(BN)_x$ ($0 \leq x \leq 1$) monolayer configurations with the unit cell sizes from 2 to 6, shown in Figure 2d. The train error and test error are 4.23 and 4.26 meV/atom, respectively, revealing the transferability of our model for the multicomponent materials.

In most cases, the fitting can be improved by increasing the number of parameters, and selecting the key parameters will enhance the efficiency. The error for the $C_{1-x}B_x$ monolayers is 9.31 and 3.05 meV/atom with 8 and 208 parameters, respectively (classifying atomic motifs by the NN and NNN environment), indicating the atomic distributions of next-nearest neighbors are dominant to total energies. Figure 3a shows the dependence of energy parameters (with the NNN cut-off) as a function of the Hirshfeld charges of the C atoms, where there is approximately a linear dependence of parameters on the charges for each C group with the NN cut-off. Considering the next-nearest neighbors, there are 16 or 36 more kinds of atoms (S_j^i) for each one of eight groups (F^i , i.e., B/C-1,2,3,4 shown in Figure 2a) with the NN cut-off, where S_j^i means the j -th kind of atom derived from the same i -th kind of atom F^i . We can introduce a vector of N , where $N_j = 0$ indicates that $S_j^i = F^i$ and $N_j = 1$ for $S_j^i \neq F^i$. In such a case, there are 2^{208} kinds of possible parameter selections, and we have employed a Monte Carlo tree search method^{34,35} to reduce the number of parameters in the energy model.

Taking $N_j = 0$, $j \in [1, 208]$ as the first layer of the Monte Carlo tree, we can randomly choose $N_j = 1$ to obtain the second layer. Similarly, all the layers of tree can be obtained by adding $N_j = 1$ from the above layer. For a given vector of N , we can calculate all cross-validation error ($E_{\text{error}}^{\text{CV}}$), where the branches in the next layer of tree are expanded, according to

the probability in proportion of $P = \exp(-E_{\text{error}}^{\text{CV}}/T)$. The parameter T is used to balance the width and depth of the search, which will decrease in the search process to find the optimum combination of parameters. The fitting is gradually improved as the number of parameters increases, and the cross-validation errors are minimized with given number of parameters from 15 to 200. As shown in Figure 3b, we can use only 50 parameters to obtain a good fitting with the cross-validation mean absolute error of 4.04 meV/atom of the 17 010 configurations data set. Based on the cluster expansion,²¹ the cross-validation error was found to be 6 meV/atom, using a data set of 307 structures.

Figure 3(c) shows the parameters for B/C-centered motifs with various bonding environments. The C-centered parameters will increase as the number of B atoms increases, which indicates that the B-doping on a perfect graphene will be less stable as the number of carbon decreases. Meanwhile, the B-centered parameters will decrease as the number of C atoms increases, which is also self-consistent in our model. According to the C-centered substructures (shown in Figure 3d), we can conclude that the B atoms tend to be far away from each other (marked in blue) because the clustering of B atoms will induce considerable positive contributions to the total energy (marked in red). Thus, the energy parameters in ACM will give a better understanding of the structural stabilities of $C_{1-x}B_x$ monolayers.

In the following, we will demonstrate that the key atomic motifs with specific bonding environment can describe the structural evolution as a function of temperature. The total energies can be accurately estimated with ACM in an efficient way, and the phase transition can be further studied with the Monte Carlo simulation. Taking the C_3B phase as an example, we have constructed a $C_{180}B_{60}$ hexagonal monolayer with random distributions of B and C atoms, with temperature annealed from 6000 to 50 K, and 10^6 Monte Carlo steps are used at each iteration to ensure the thermal equilibrium. The probabilities of motifs are found to evolve with the temperature, as shown in the Figure 4a. At high temperature, the probabilities of motifs are even, which corresponds to the random distribution of B/C atoms. As the temperature decreases, two B/C-centered motifs become dominant (shown in Figure 4b), which will compose the order structure of C_3B . Thus, the probability distributions of motifs can serve as the order parameter in the order–disorder phase process, distinguishing the local characteristic of motifs.

For the $C_{1-2x}(BN)_x$ monolayers, the previous study showed the critical temperature of complete miscibility around 3500 K.²¹ Herein, we have constructed a $C_{120}B_{60}N_{60}$ hexagonal monolayer to study the structural evolution under various temperatures. The total energies are estimated by ACM with the NN cut-off, and 10^6 Monte Carlo steps have been taken for the thermodynamic equilibrium. As shown in Figure 5, there is a clear phase separation in the stable structure of heterographene at low temperature. The system will become miscible when the temperature increases from 0 to 5000 K, where the regions of complete graphene and BN vanish gradually. With the NN cut-off, we have determined 30 nonduplicated motifs, whose variation of probabilities shows a clear picture of the phase transition. At low temperature, there are three C atoms at the nearest neighbors for most C atoms, and B/N atoms are energetically preferable at the nearest neighbors of N/B atoms. Thus, there are three motifs (7th, 20th, and 21st) with high probabilities of ensemble average.

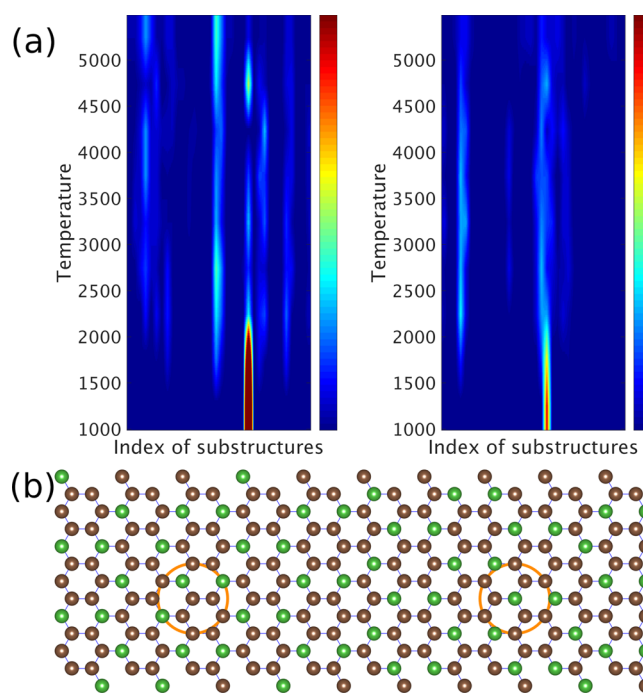


Figure 4. Structural evolution of C_3B : (a) the probabilities of C/B-centered motifs; (b) the ordered structure of C_3B and the key motifs are marked with the two circles.

With the increasing of temperature, there is a dramatical decrease in the probabilities of 20th and 21st motifs, with the vanishing of BN region. The sites in the $C_{120}B_{60}N_{60}$ system will be randomly occupied by B/C/N atoms,³⁶ therefore, the 5th, 18th, and 26th motifs, which satisfy $n_B/n_N/n_C = 1:1:2$, will be of high probability at high temperature. The probability of 7th motif is also decreased while that of the 5th one is increased, indicating that two outer C atoms of 7th motif are gradually replaced by B and N atoms. The probabilities of all motifs are calculated at high temperature limit (plot in red), which is in agreement with the results of Monte Carlo simulation at $T = 4800$ K.

Analogous to Special Quasirandom Structures,³⁶ we have obtained the representative structures based on the motif probability with the frame of ACM. Figure 6 shows the electronic band structures of the representative structures at ensemble equilibrium with various temperatures. The primitive cells are used for the ordered structures at $T = 0$ K, and the supercells are used for high temperature. $C_{180}B_{60}$ is semiconducting with the gap of 0.543 eV at $T = 0$ K, and the band gap will vanish with the increasing of temperature. Drastic atomic exchange because of high temperature will significantly influence the atomic distribution, which causes the transition from the semiconductor to metal. For $C_{120}B_{60}N_{60}$, it is semimetallic at $T = 0$ K. At higher temperature, the $C_{120}B_{60}N_{60}$ structures will become metallic because of the irregular atomic distribution.

CONCLUSIONS

In summary, we have proposed an ACM to describe the structural stabilities, where the test error of the $C_{1-x}B_x$ and $C_{1-2x}(BN)_x$ monolayers is only 3 meV. Note that the parameters in our model have a positive correlation with charge distribution and the number of parameters can be further reduced maintaining the good accuracy. The key motifs

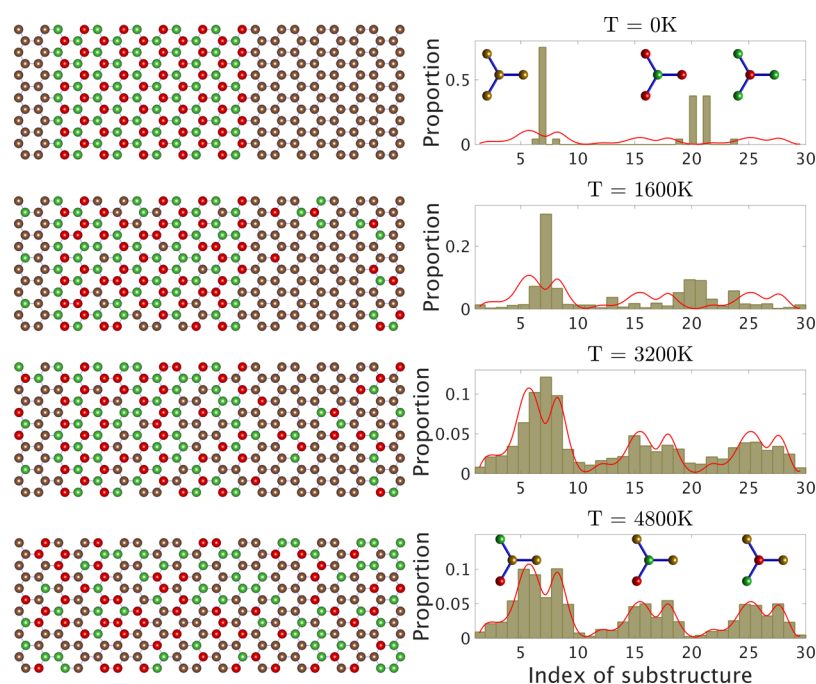


Figure 5. Typical configurations $C_{120}B_{60}N_{60}$ under various temperatures and histogram of substructures with different temperatures. The probabilities of all motifs at high-temperature limit are plotted in red lines.

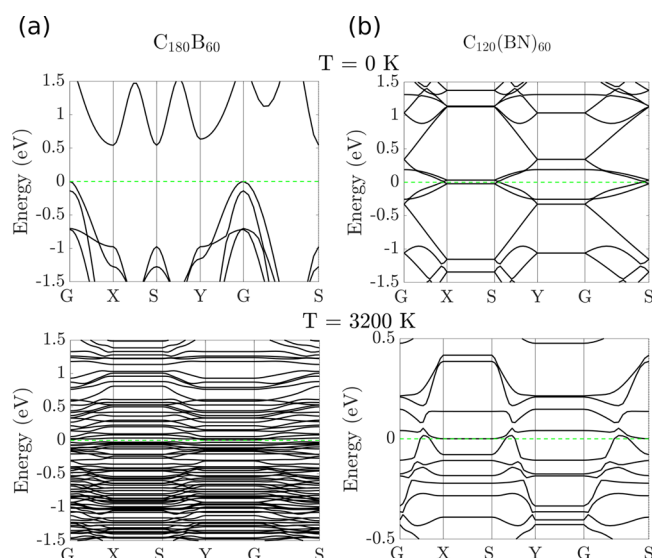


Figure 6. Electronic band structures of representative structures for: (a) $C_{180}B_{60}$; (b) $C_{120}(BN)_{60}$ at specific temperatures.

will facilitate the searching of stable structures and serve as the order parameters to provide a clear picture of structural evolution at various temperatures.

AUTHOR INFORMATION

Corresponding Author

Xiao-Bao Yang – Department of Physics, South China University of Technology, Guangzhou 510640, China; orcid.org/0000-0001-8851-1988; Email: scxbyang@scut.edu.cn

Authors

Chang-Chun He – Department of Physics, South China University of Technology, Guangzhou 510640, China

Shao-Bin Qiu – Department of Physics, South China University of Technology, Guangzhou 510640, China

Ju-Song Yu – Department of Physics, South China University of Technology, Guangzhou 510640, China

Ji-Hai Liao – Department of Physics, South China University of Technology, Guangzhou 510640, China; State Key Laboratory of Metastable Materials Science and Technology, Yanshan University, Qinhuangdao 066004, China

Yu-Jun Zhao – Department of Physics, South China University of Technology, Guangzhou 510640, China; orcid.org/0000-0002-6923-1099

Complete contact information is available at:

<https://pubs.acs.org/10.1021/acs.jpca.0c02431>

Notes

The authors declare no competing financial interest.

ACKNOWLEDGMENTS

This work was supported by Guangdong Natural Science Funds for Distinguished Young Scholars (no. 2014A030306024) and for Doctoral Program (grant no. 2017A030310086), National Natural Science Foundation of China (nos. 11474100, U1601212), and the Fundamental Research Funds for the Central Universities (no. 2018ZD46).

REFERENCES

- (1) Xu, M.; Liang, T.; Shi, M.; Chen, H. Graphene-like two-dimensional materials. *Chem. Rev.* **2013**, *113*, 3766–3798.
- (2) Zeng, M.; Xiao, Y.; Liu, J.; Yang, K.; Fu, L. Exploring two-dimensional materials toward the next-generation circuits: from monomer design to assembly control. *Chem. Rev.* **2018**, *118*, 6236–6296.
- (3) Chen, Y.; Fan, Z.; Zhang, Z.; Niu, W.; Li, C.; Yang, N.; Chen, B.; Zhang, H. Two-dimensional metal nanomaterials: synthesis, properties, and applications. *Chem. Rev.* **2018**, *118*, 6409–6455.

- (4) Novoselov, K. S.; Geim, A. K.; Morozov, S. V.; Jiang, D.; Zhang, Y.; Dubonos, S. V.; Grigorieva, I. V.; Firsov, A. A. Electric field effect in atomically thin carbon films. *Science* **2004**, *306*, 666–669.
- (5) Zhang, Y.; Tan, Y.-W.; Stormer, H. L.; Kim, P. Experimental observation of the quantum Hall effect and Berry's phase in graphene. *Nature* **2005**, *438*, 201–204.
- (6) Qian, X.; Liu, J.; Fu, L.; Li, J. Quantum spin Hall effect in two-dimensional transition metal dichalcogenides. *Science* **2014**, *346*, 1344–1347.
- (7) Saito, Y.; Nojima, T.; Iwasa, Y. Highly crystalline 2D superconductors. *Nat. Rev. Mater.* **2016**, *2*, 16094.
- (8) Cao, Y.; Fatemi, V.; Fang, S.; Watanabe, K.; Taniguchi, T.; Kaxiras, E.; Jarillo-Herrero, P. Unconventional superconductivity in magic-angle graphene superlattices. *Nature* **2018**, *556*, 43–50.
- (9) Zhou, J.; Lin, J.; Huang, X.; Zhou, Y.; Chen, Y.; Xia, J.; Wang, H.; Xie, Y.; Yu, H.; Lei, J.; et al. A library of atomically thin metal chalcogenides. *Nature* **2018**, *556*, 355–359.
- (10) Park, C.-H.; Louie, S. G. Energy gaps and stark effect in boron nitride nanoribbons. *Nano Lett.* **2008**, *8*, 2200–2203.
- (11) Golberg, D.; Bando, Y.; Huang, Y.; Terao, T.; Mitome, M.; Tang, C.; Zhi, C. Boron nitride nanotubes and nanosheets. *ACS Nano* **2010**, *4*, 2979–2993.
- (12) Muchharla, B.; Pathak, A.; Liu, Z.; Song, L.; Jayasekera, T.; Kar, S.; Vajtai, R.; Balicas, L.; Ajayan, P. M.; Talapatra, S.; et al. Tunable electronics in large-area atomic layers of boron-nitrogen-carbon. *Nano Lett.* **2013**, *13*, 3476–3481.
- (13) Liu, Z.; Ma, L.; Shi, G.; Zhou, W.; Gong, Y.; Lei, S.; Yang, X.; Zhang, J.; Yu, J.; Hackenberg, K. P.; et al. In-plane heterostructures of graphene and hexagonal boron nitride with controlled domain sizes. *Nat. Nanotechnol.* **2013**, *8*, 119–124.
- (14) Lu, J.; Zhang, K.; Feng, L.; Zhang, H.; Chien, S.; Sum, T.; Castro Neto, A. H.; Loh, K. P. Order-disorder transition in a two-dimensional boron-carbon-nitride alloy. *Nat. Commun.* **2013**, *4*, 2681.
- (15) Jones, R. O. Density functional theory: Its origins, rise to prominence, and future. *Rev. Mod. Phys.* **2015**, *87*, 897–923.
- (16) Jain, A.; Hautier, G.; Moore, C. J.; Ping Ong, S.; Fischer, C. C.; Mueller, T.; Persson, K. A.; Ceder, G. A high-throughput infrastructure for density functional theory calculations. *Comput. Mater. Sci.* **2011**, *50*, 2295–2310.
- (17) Curtarolo, S.; Hart, G. L. W.; Nardelli, M. B.; Mingo, N.; Sanvito, S.; Levy, O. The high-throughput highway to computational materials design. *Nat. Mater.* **2013**, *12*, 191–201.
- (18) Jóhannesson, G. H.; Bligaard, T.; Ruban, A. V.; Skriver, H. L.; Jacobsen, K. W.; Nørskov, J. K. Combined electronic structure and evolutionary search approach to materials design. *Phys. Rev. Lett.* **2002**, *88*, 255506.
- (19) van de Walle, A. A complete representation of structure-property relationships in crystals. *Nat. Mater.* **2008**, *7*, 455–458.
- (20) Hart, G. L. W.; Blum, V.; Walorski, M. J.; Zunger, A. Evolutionary approach for determining first-principles hamiltonians. *Nat. Mater.* **2005**, *4*, 391–394.
- (21) Yuge, K. Phase stability of boron carbon nitride in a heterographene structure: A first-principles study. *Phys. Rev. B: Condens. Matter Mater. Phys.* **2009**, *79*, 144109.
- (22) Zhang, M.; Gao, G.; Kutana, A.; Wang, Y.; Zou, X.; Tse, J. S.; Yakobson, B. I.; Li, H.; Liu, H.; Ma, Y. Two-dimensional boron-nitrogen-carbon monolayers with tunable direct band gaps. *Nanoscale* **2015**, *7*, 12023–12029.
- (23) Krepel, D.; Hod, O. Effects of edge oxidation on the structural, electronic, and magnetic properties of zigzag boron nitride nanoribbons. *J. Chem. Theory Comput.* **2014**, *10*, 373–380.
- (24) Harrison, J. F. A Hirshfeld-I interpretation of the charge distribution, dipole and quadrupole moments of the halogenated acetylenes FCCH, ClCCH, BrCCH, and ICCH. *J. Chem. Phys.* **2010**, *133*, 214103.
- (25) Kresse, G.; Hafner, J. Ab initio molecular dynamics for open-shell transition metals. *Phys. Rev. B: Condens. Matter Mater. Phys.* **1993**, *48*, 13115–13118.
- (26) Kresse, G.; Furthmüller, J. Efficient iterative schemes for ab initio total-energy calculations using a plane-wave basis set. *Phys. Rev. B: Condens. Matter Mater. Phys.* **1996**, *54*, 11169–11186.
- (27) Kresse, G.; Joubert, D. From ultrasoft pseudopotentials to the projector augmented-wave method. *Phys. Rev. B: Condens. Matter Mater. Phys.* **1999**, *59*, 1758–1775.
- (28) Perdew, J. P.; Burke, K.; Ernzerhof, M. Generalized gradient approximation made simple. *Phys. Rev. Lett.* **1996**, *77*, 3865–3868.
- (29) Structures of Alloys Generation And Recognition. <http://sagar.compphys.cn/sagar> (accessed 2020-05-14).
- (30) Hart, G. L. W.; Forcade, R. W. Algorithm for generating derivative structures. *Phys. Rev. B: Condens. Matter Mater. Phys.* **2008**, *77*, 224115.
- (31) Li, X.-T.; Yang, X.-B.; Zhao, Y.-J. Geometrical eigen-subspace framework based molecular conformation representation for efficient structure recognition and comparison. *J. Chem. Phys.* **2017**, *146*, 154108.
- (32) Cheng, Y. H.; Liao, J. H.; Zhao, Y. J.; Yang, X. B. An extended cluster expansion for ground states of heterofullerenes. *Sci. Rep.* **2017**, *7*, 16211.
- (33) Schmidhuber, J. Deep learning in neural networks: An overview. *Neural Network.* **2015**, *61*, 85–117.
- (34) Frontera, C.; Vives, E.; Castán, T.; Planes, A. Monte Carlo simulation of interface alloying. *Phys. Rev. B: Condens. Matter Mater. Phys.* **1995**, *51*, 11369–11375.
- (35) Cao, Z.-P.; Zhao, Y.-J.; Liao, J.-H.; Yang, X.-B. Gap maximum of graphene nanoflakes: a first-principles study combined with the Monte Carlo tree search method. *RSC Adv.* **2017**, *7*, 37881–37886.
- (36) Zunger, A.; Wei, S.-H.; Ferreira, L. G.; Bernard, J. E. Special quasirandom structures. *Phys. Rev. Lett.* **1990**, *65*, 353–356.